Crow Instability

Arthur Shiniti Cato, Pedro Morel Rosa, and Pietro Tanure Onnis

Introduction to Hydrodynamic Instabilities

Abstract:

The Crow instability is studied to demonstrate the applicability of linear instability theory. The Finite Element Method and a non-linear Euler time-stepping are used to perform a DNS simulation of the evolution of two counter-rotating Lamb-Oseen vortices. A quasi-static flow is approximated from the unsteady solution and the eigenvalue problem is derived from the dispersion relation of the perturbation modes. The most unstable modes are computed and compared to the literature. The numerical results were obtained with the use of *FEniCS*.

Keywords: Crow instability; linear stability; counter-rotating vortices, aerodynamics; fluid mechanics

---

This document has pedagogical purposes and its objective is to use the knowledge acquired from the lectures in a practical context.

1 Introduction

Instability theory plays an important role to characterize fluid dynamics. The complex behaviour of an unstable system (or marginally stable) can be difficult to understand and mathematically demanding to model. Nevertheless, they are crucial to engineering and applied sciences, being of both practical and theoretical importance.

In addition to describe unstable phenomena, the instability theory also focuses on clarifying the limits of the stable and unstable domains. In other words, it helps to predict the conditions of stability.

Several instabilities are still under research in fluid dynamics, although there are some classical examples which were the foundations where the theory was established. Some examples are: Kelvin-Helmholtz instability, Rayleigh-Taylor instability, Plateau-Rayleigh etc.

This document presents to the reader a brief study of the so called Crow instability. The aim of this study is to use some of the basic mathematical tools of the instability theory to demonstrate its capabilities and to create an interesting pedagogical material.

The work presents the simulation of the base flow with the main assumptions and tools used, followed by the linear instability analysis and results provided by it. It ends with a brief comparison with the literature.

1.1 Crow Instability

In the wingtips of an aircraft a pair of counter-rotating vortices are generated and travels behind the aircraft. The trailing vortices of heavy airplanes can persist enough time to cause dangerous disturbances in the air to lighter airplanes that flies in the same zone.

These structures interact with one another. As the disturbances in the longitudinal direction get amplified, the trails undergo a slow, symmetric and sinusoidal instability [2].

One of the interesting features of these structures is that they can interact with each other until collapse forming a ring chain. This process is called Crow instability and it was first explored by S. C. Crow (1970) [2].

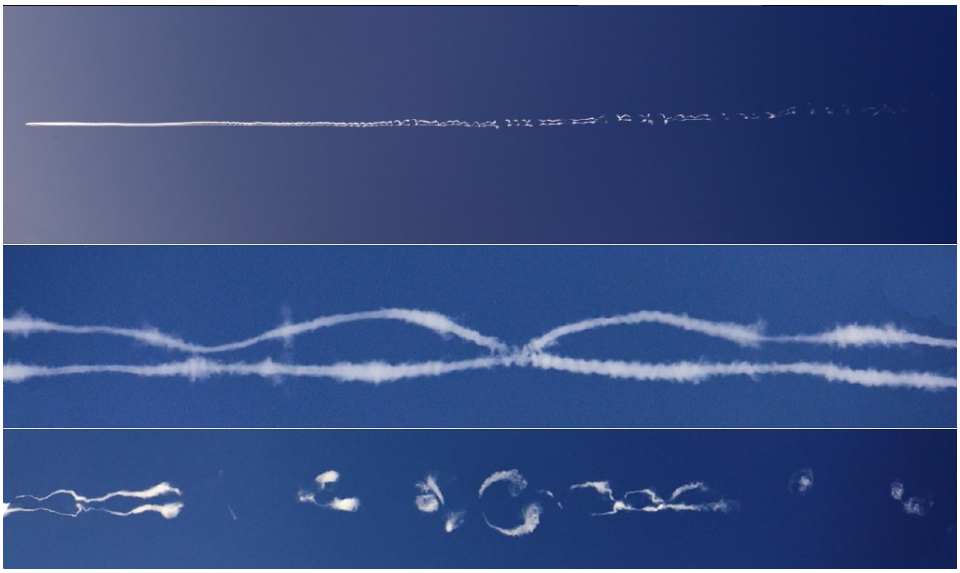

Figura 1: Crow instability on trailing vortexes of airplanes (Image featured by NASA: Earth Science Picture of the Day on August 9, 2011.)

If this instability was not present the vortex trails would last for much more time as the simple diffusion process is very slow compared to the perturbations [2].

2 Base Flow

For the instability analysis it is necessary to define a base flow solution.

The base flow to be considered is a two-dimensional pair of counter-rotating vortices initially modelled as Lamb-Oseen vortices. The flow is assumed to be homogeneous in the longitudinal direction (z-direction) and it is symmetric with respect to $x = 0$. Cartesian coordinates are used (x, y, z).

Each Lamb-Oseen vortex can be modelled by the equation:

$$V_\theta(r) = \frac{\Gamma}{2\pi r}\left[1 - exp\left(-\frac{r^2}{a^2}\right)\right] \tag{1}$$

Where a is the mean radius of the vortex and Γ is the vortex circulation.

The physical phenomenon is time-dependent, however a time scale analysis indicates that the problem can be approximated to a steady-state flow to study stability, as suggested by Brion, Sipp and Jacquin (2007) [1].

One can consider that two different time scales are presented: the time associated to the natural diffusion of the vortices and the characteristic time of the perturbations. The time scales for the viscous diffusion and the perturbations of the crow instability are given respectively by:

$$T_\nu \approx \frac{2\pi a^2}{\nu} \qquad T_p \approx \frac{2\pi b^2}{\Gamma} \tag{2}$$

Where b is the distance between the center of the two vortices and a is the mean radius. The ratio between these two time-scales is given by equation (3).

$$\frac{T_\nu}{T_p} \approx Re\left(\frac{a}{b}\right)^2 \tag{3}$$

The ratio of the time scales increases with the Re number. For sufficient large Re one can consider the flow quasi-static with respect to the perturbations. This assumption is used to perform the linear instability analysis.

2.1 Numerical implementation

As discussed previously, the unsteady problem can be approximated to a quasi-static one, however, a DNS simulation is performed in order to have a Navier-Stokes solution for the base flow. The initial condition is given by two Lamb-Oseen vortices in counter rotation and the symmetry of the problem allows the computational domain to be reduced in half.

The left, down and upper boundaries are stress-free and no flux is imposed on the symmetry plane. The velocity of the vortices in the vertical direction is given by $2\pi b/\Gamma$ [1] and the negative of this value is added to the velocity field to ensure a steady referential frame.

The Finite Element Method is used to perform the simulation with a non-linear Euler time-stepping. The code uses the open-source package *FEniCS* and the unstructured mesh was created with the open-source software *Gmsh*. A brief mesh convergence study was done for the time-dependent simulations using the meshes in Fig. 2. It was seen that the results did not change in practice, thus the intermediate mesh was chosen to provide a balance between computational cost and accuracy.

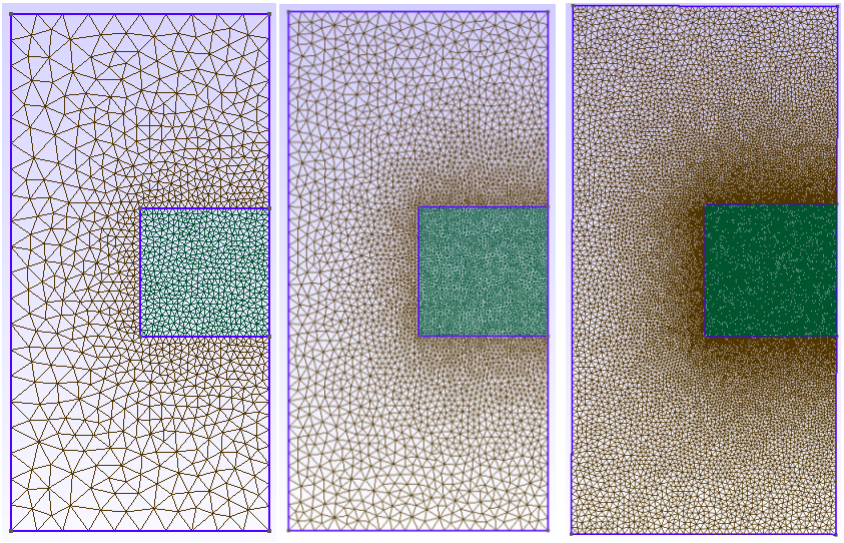

Figura 2: Meshes tested with refinement level of resolution r=0.5; r=0.025 and r=0.0125 respectively. The mesh with r=0.025 was chosen for the rest of the study.

For the DNS simulation the Kolmogorov scale of diffusion needs to be considered, consequently, the discretization needs to be at least $\eta/L = Re^{-3/4}$. Since the problem is 2D the number of elements per area of characteristic length (L^2) is $(L/\eta)^2 = Re^{6/4} = 100^{6/4} = 1000$. The characteristic length considered for the DNS simulation is the average size a of the vortex. The time discretization is also determined by the Kolmogorov scale $\tau_L/\tau_\eta = Re^{1/2}$. After running for 1 second in simulation time, the observed result is given by Figures 3 and 4. Figure 3 shows the streamlines closed to the core of the vortices; as expected according to [1], they have oval shapes with two hyperbolic points in the top and bottom of the image.

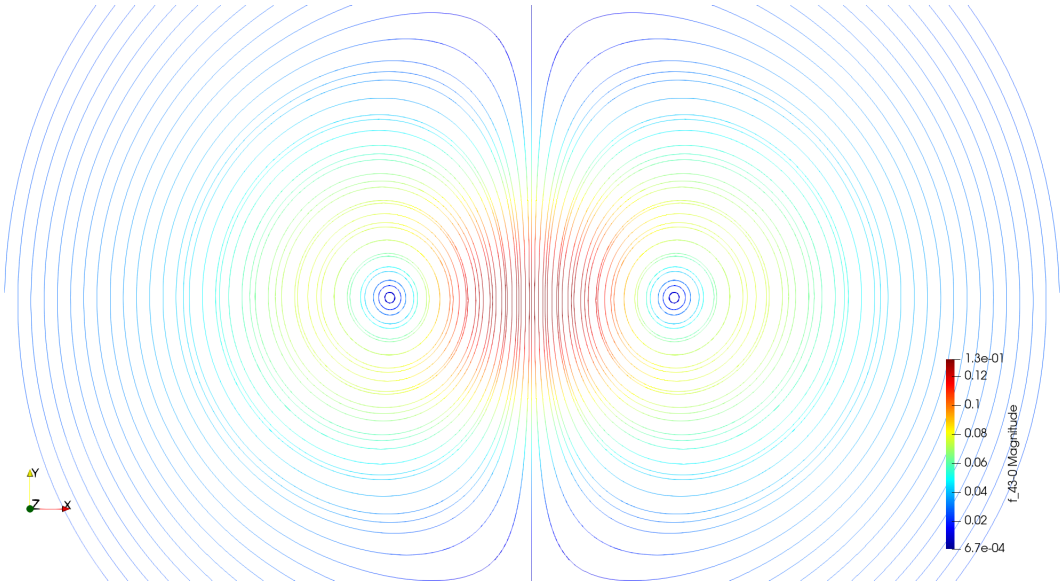

Figura 3: Streamlines of the solution

Figure 4 show the whole domain (with reflection of the symmetric half) with the elements of the mesh explicit. One can see that near the core of the cortex, where the velocity gradients are higher, the mesh is more refined.

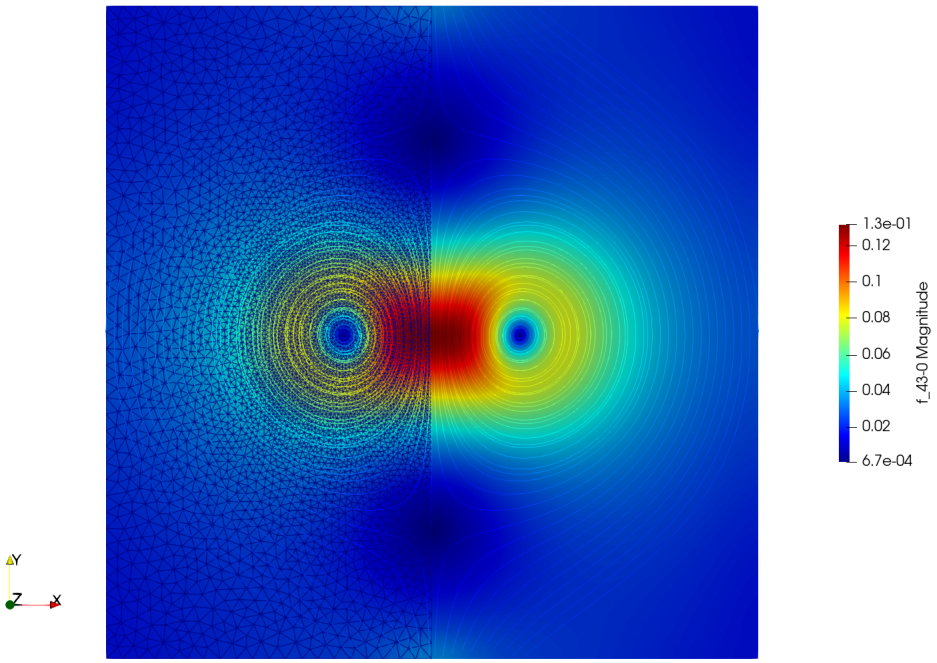

Figura 4: Solution of the full domain

3 Stability Analysis

The linear stability analysis is performed over the base flow computed previously. For this problem, the perturbations have a wave form in the z-direction and the associated wave number k is imposed. The dispersion relation gives the complex frequencies through the solution of an eigenvalue problem. As it is further explained, the complex frequency can indicate the unstable modes.

To derive the instability problem, one can consider the incompressible Navier-Stokes equations (4).

$$\begin{aligned} \partial_t \mathbf{u} + (\mathbf{u} \cdot \nabla)\, \mathbf{u} + \nabla p - \mathrm{Re}^{-1} \Delta \mathbf{u} = 0 \\ \nabla \cdot \mathbf{u} = 0 \end{aligned} \tag{4}$$

In order to develop the linear stability theory it is assumed that a small perturbation $(\mathbf{u}', p')$ is applied over the base flow characterized by the velocity and pressure fields $(\mathbf{U}, P)$ as written in (5).

$$\begin{aligned} \mathbf{u} &= \mathbf{U} + \varepsilon \mathbf{u}' \\ p &= P + \varepsilon p' \end{aligned} \tag{5}$$

The expanded field is introduced in the Navier-Stokes equations:

$$\begin{aligned} \partial_t \mathbf{U} + \varepsilon \partial_t \mathbf{u}' + (\mathbf{U} \cdot \nabla)\, \mathbf{U} + \varepsilon\, (\mathbf{U} \cdot \nabla)\, \mathbf{u}' + \varepsilon\, (\mathbf{u}' \cdot \nabla)\, \mathbf{U} + \varepsilon^2\, (\mathbf{u}' \cdot \nabla)\, \mathbf{u}' + \\ + \nabla P + \varepsilon \nabla p' - \mathrm{Re}^{-1} \Delta \mathbf{U} - \varepsilon \mathrm{Re}^{-1} \Delta \mathbf{u}' = 0 \\ \nabla \cdot \mathbf{U} + \varepsilon \nabla \cdot \mathbf{u}' = 0 \end{aligned} \tag{6}$$

If one neglects the high order terms and since the base flow is solution of the Navier-Stokes equation, equation (6) is simplified to equation (7).

$$\begin{aligned} \varepsilon \partial_t \mathbf{u}' + \varepsilon\, (\mathbf{U} \cdot \nabla)\, \mathbf{u}' + \varepsilon\, (\mathbf{u}' \cdot \nabla)\, \mathbf{U} + \varepsilon \nabla p' - \varepsilon \mathrm{Re}^{-1} \Delta \mathbf{u}' = 0 \\ \varepsilon \nabla \cdot \mathbf{u}' = 0 \end{aligned} \tag{7}$$

Or written in components:

$$\begin{aligned}
\partial_t u' + U\partial_x u' + V\partial_y u' + u'\partial_x U + v'\partial_y U + \partial_x p' - \mathrm{Re}^{-1}\left(\partial_{xx}u' + \partial_{yy}u' + \partial_{zz}u'\right) = 0 \\
\partial_t v' + U\partial_x v' + V\partial_y v' + u'\partial_x V + v'\partial_y V + \partial_y p' - \mathrm{Re}^{-1}\left(\partial_{xx}v' + \partial_{yy}v' + \partial_{zz}v'\right) = 0 \\
\partial_t w' + U\partial_x w' + V\partial_y w' + \partial_z p' - \mathrm{Re}^{-1}\left(\partial_{xx}w' + \partial_{yy}w' + \partial_{zz}w'\right) = 0 \\
\partial_x u' + \partial_y v' + \partial_z w' = 0
\end{aligned} \tag{8}$$

The perturbations can be expressed by its normal modes. It is important to highlight that the dependency in the z-direction (in which the base flow is homogeneous) is prescribed as a wave like form with wave number k. The form of the perturbations is as follows:

$$\mathbf{q}'\left(x, y, z, t\right) = \hat{\mathbf{q}}\left(x, y\right) e^{ikz - i\omega t} \tag{9}$$

Where the amplitudes are:

$$\hat{\mathbf{q}}\left(x, y\right) = \left(\hat{u}, \hat{v}, \hat{w}, \hat{p}\right)\left(x, y\right) \tag{10}$$

And the complex frequency is defined as:

$$\omega = \omega_r + i\omega_i \tag{11}$$

One can notice that the imaginary part of the complex frequency is multiplied by the imaginary unity twice when in equation (9), representing the growth rate of the mode.

The operators of derivative are re-written as:

$$\begin{aligned}
\partial_t &\rightarrow -i\omega \\
\partial_z &\rightarrow ik
\end{aligned} \tag{12}$$

And equation (8) becomes:

$$\begin{aligned}
-i\omega\hat{u} + U\partial_x\hat{u} + V\partial_y\hat{u} + \hat{u}\partial_x U + \hat{v}\partial_y U + \partial_x\hat{p} - \mathrm{Re}^{-1}\left(\partial_{xx}\hat{u} + \partial_{yy}\hat{u} - k^2\hat{u}\right) = 0 \\
-i\omega\hat{v} + U\partial_x\hat{v} + V\partial_y\hat{v} + \hat{u}\partial_x V + \hat{v}\partial_y V + \partial_y\hat{p} - \mathrm{Re}^{-1}\left(\partial_{xx}\hat{v} + \partial_{yy}\hat{v} - k^2\hat{v}\right) = 0 \\
-i\omega\hat{w} + U\partial_x\hat{w} + V\partial_y\hat{w} + \partial_z\hat{p} - \mathrm{Re}^{-1}\left(\partial_{xx}\hat{w} + \partial_{yy}\hat{w} - k^2\hat{w}\right) = 0 \\
\partial_x\hat{u} + \partial_y\hat{v} + ik\hat{w} = 0
\end{aligned} \tag{13}$$

Or (in a more suggestive form):

$$\begin{aligned}
-i\omega\hat{u} = -U\partial_x\hat{u} - V\partial_y\hat{u} - \hat{u}\partial_x U - \hat{v}\partial_y U - \partial_x\hat{p} + \mathrm{Re}^{-1}\left(\partial_{xx}\hat{u} + \partial_{yy}\hat{u} - k^2\hat{u}\right) \\
-i\omega\hat{v} = -U\partial_x\hat{v} - V\partial_y\hat{v} - \hat{u}\partial_x V - \hat{v}\partial_y V - \partial_y\hat{p} + \mathrm{Re}^{-1}\left(\partial_{xx}\hat{v} + \partial_{yy}\hat{v} - k^2\hat{v}\right) \\
-i\omega\hat{w} = -U\partial_x\hat{w} - V\partial_y\hat{w} - \partial_z\hat{p} + \mathrm{Re}^{-1}\left(\partial_{xx}\hat{w} + \partial_{yy}\hat{w} - k^2\hat{w}\right) \\
0 = \partial_x\hat{u} + \partial_y\hat{v} + ik\hat{w}
\end{aligned} \tag{14}$$

The set of equations (14) is an eigenvalue problem.

$$-i\omega B\hat{\mathbf{q}} = A\hat{\mathbf{q}} \tag{15}$$

Which can be expressed in the following matrix form:

$$\mathbf{A} = \begin{bmatrix}
-\mathcal{C} - \partial_x U + \mathcal{V} & -\partial_y U & 0 & -\partial_x \\
-\partial_x V & -\mathcal{C} - \partial_y V + \mathcal{V} & 0 & -\partial_y \\
0 & 0 & -\mathcal{C} + \mathcal{V} & -ik \\
\partial_x & \partial_y & ik & 0
\end{bmatrix} \tag{16}$$

Where $\mathcal{C} = U\partial_x + V\partial_y$ is the convective term and $\mathcal{V} = 1/Re\left(\partial_{xx} + \partial_{yy} - k^2\right)$ is the viscous one.

The aim is to solve the eigenvalue problem (EVP) to find the most unstable modes, which are the ones with positive growth rate in time. Due to the way the expressions were defined, these modes have positive imaginary part of their frequency.

3.1 Weak formulation

The resulting matrix of the EVP is associated to a non-parallel flow and considered too large for a full eigenmode decomposition. For this reason, a shift value σ is chosen to compute its closest eigenvalues.

A finite element method is chosen to compute the matrix system and the weak formulation of the set (14) is derived. The vector **v** represents the test functions and integration by parts is performed for the pressure and viscous terms. The boundaries has stress-free conditions and the integrated terms are cancelled there.

For the x-direction:

$$\begin{gathered}\int_\Omega \left[-i\omega\hat{u} + U\partial_x\hat{u} + V\partial_y\hat{u} + \hat{u}\partial_x U + \hat{v}\partial_y U + \partial_x\hat{p} - \mathrm{Re}^{-1}\left(\partial_{xx}\hat{u} + \partial_{yy}\hat{u} - k^2\hat{u}\right)\right] v_x d\Omega = 0 \Rightarrow \\ \int_\Omega \left[-i\omega\hat{u} + U\partial_x\hat{u} + V\partial_y\hat{u} + \hat{u}\partial_x U + \hat{v}\partial_y U + \hat{p}\partial_x v_x - \mathrm{Re}^{-1}\left(grad\left(\hat{u}\right) grad\left(v_x\right) - k^2\right)\right] v_x d\Omega = 0\end{gathered} \tag{17}$$

For the y-direction:

$$\begin{gathered}\int_\Omega \left[-i\omega\hat{v} + U\partial_x\hat{v} + V\partial_y\hat{v} + \hat{u}\partial_x V + \hat{v}\partial_y V + \partial_y\hat{p} - \mathrm{Re}^{-1}\left(\partial_{xx}\hat{v} + \partial_{yy}\hat{v} - k^2\hat{v}\right)\right] v_y d\Omega = 0 \Rightarrow \\ \int_\Omega \left[-i\omega\hat{v} + U\partial_x\hat{v} + V\partial_y\hat{v} + \hat{u}\partial_x V + \hat{v}\partial_y V + \hat{p}\partial_y v_y - \mathrm{Re}^{-1}\left(grad\left(\hat{v}\right) grad\left(v_y\right) - k^2\right)\right] v_y d\Omega = 0\end{gathered} \tag{18}$$

And for the z-direction:

$$\begin{gathered}\int_\Omega \left[-i\omega\hat{w} + U\partial_x\hat{w} + V\partial_y\hat{w} + \partial_z\hat{p} - \mathrm{Re}^{-1}\left(\partial_{xx}\hat{w} + \partial_{yy}\hat{w} - k^2\hat{w}\right)\right] v_z d\Omega = 0 \Rightarrow \\ \int_\Omega \left[-i\omega\hat{w} + U\partial_x\hat{w} + V\partial_y\hat{w} + \hat{p}\partial_z v_z - \mathrm{Re}^{-1}\left(grad\left(\hat{w}\right) grad\left(v_z\right) - k^2\right)\right] v_z d\Omega = 0\end{gathered} \tag{19}$$

Once the weak formulation of the problem is derived, the EVP is solved with respect to the shift value.

4 Results

Given the analytical and numerical developments presented in the previous sections of this work, it was possible to analyze the instabilities of the proposed phenomenon.

Among the conditions chosen for the analysis, the Reynolds number selected was Re = 100 and the results were obtained after 1s of base flow simulation. The first 10 eigenmodes were chosen for the analysis and, among them, the value with the highest magnitude was selected. This analysis covered values of wavelength k from 0 to 0.5. Thus, it was possible to obtain the results of Figure 5.

It is important to emphasize that our results were obtained considering a geometric ratio between the vortices mean radius a and vortices distance b of approximately $a/b \approx 0.25$. The base for the instability analysis done by Hein and Theofilis (2004) [3] was obtained by a different ratio ($a/b \approx 0.5$) and the flow was simulated in a much bigger domain in order to not have the boundary conditions interfere in the flow field. Such simulation would require more computational cost. Although the Reynolds are the same, the flow field, the a/b ratio and the time of simulated can be accounted for the difference in results.

Nevertheless, the results computed in this work show similar behaviour to the ones provided by the literature. The range of wave number where unstable modes occur are corresponding and there is an increase of the growth rate until the value followed by the decrease of the same. An additional remark is that the geometrical ratio of the present case is approximately half of the ratio used by Hein and Theofilis (2004) [3], as well as the maximum value of ω_i found in this work is half of the one in the paper.

Finally, the results obtained from Brion, Sipp and Jacquin (2007) [1], for $Re = 3600$ and $a/b = 0.2$ are shown in Figure 6. The results plotted by them were normalized according to a reference value and the way they defined the complex frequency in the perturbation modes implies that the growth rate is given by the real part rather than the imaginary. However, although different parameters were used, it is remarkable that the most unstable modes preserves some similarity in the format of the curve.

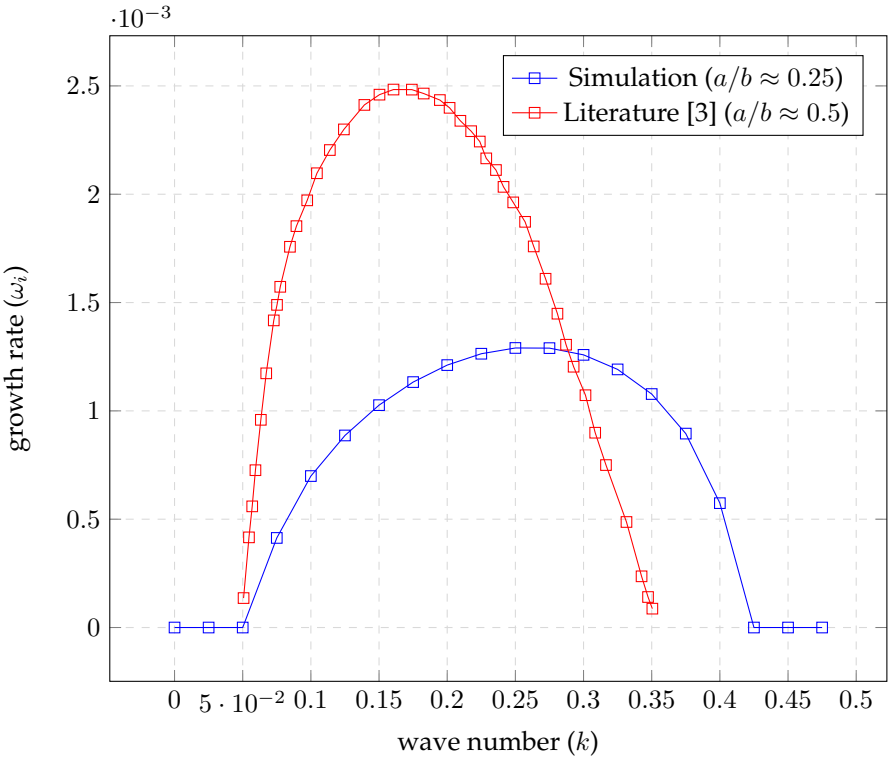

Figura 5: Wave number and growth rate

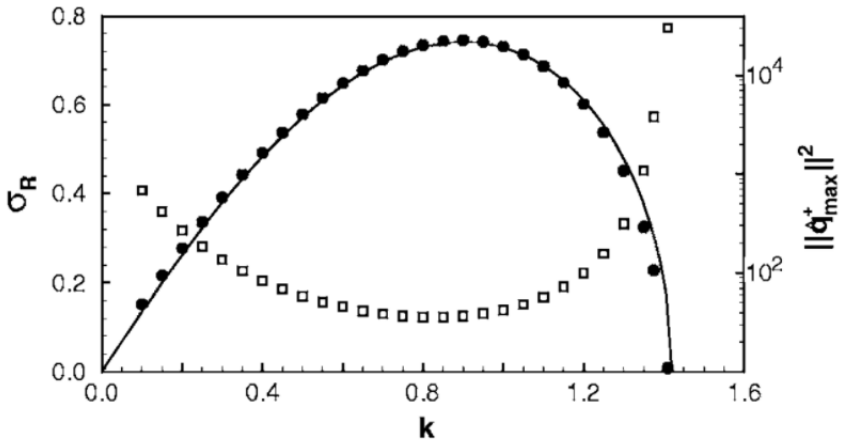

Figura 6: Normalized Wave number and growth rate for $a/b = 0.2$ and $Re = 3600$ from [1]

5 Conclusions

This work aimed to present and discuss the Crow instability. Although challenging to implement numerically given the 3D harmonic component of the disturbance variables in a 2D mesh grid, the project offered many fruitful learning opportunities in the field of numerical simulation and instability analysis, for instance the use of DNS simulation with *FEniCS*. Given the phenomenon presented and the results obtained in this study, it can be said that several agreements of a qualitative nature occurred.

Referências

[1] BRION, V., SIPP, D., AND JACQUIN, L. Optimal amplification of the crow instability. *Physics of Fluids 19* (11 2007). 10.1063/1.2793146.

[2] CROW, S. C. Stability theory for a pair of trailing vortices. *AIAA Journal 8* (1970), 2172–2179.

[3] HEIN, S., AND THEOFILIS, V. On instability characteristics of isolated vortices and models of trailing-vortex systems. *Computers Fluids 33*, 5 (2004), 741–753. https://doi.org/10.1016/j.compfluid.2003.05.004. Applied Mathematics for Industrial Flow Problems.